UNIVERSIDAD REGIONAL AMAZÓNICA IKIAM

FACULTAD DE CIENCIAS DE LA TIERRA Y AGUA

CARRERA EN GEOCIENCIAS

TOMOGRAFÍA SÍSMICA DE TIEMPO DE VIAJE PARA LA INTERPRETACIÓN SISMOESTRATIGRÁFICA DE LA CORTEZA ALREDEDOR DEL KNICKPOINT DE SAN RAFAEL EN EL RÍO COCA, ECUADOR.

Proyecto de investigación previo a la obtención del Título de:

INGENIERA EN GEOCIENCIAS

AUTOR

ISABEL CRISTINA GARCÍA LÓPEZ

Napo - Ecuador

2023

UNIVERSIDAD REGIONAL AMAZÓNICA IKIAM

FACULTAD DE CIENCIAS DE LA TIERRA Y AGUA

CARRERA EN GEOCIENCIAS

TOMOGRAFÍA SÍSMICA DE TIEMPO DE VIAJE PARA LA INTERPRETACIÓN SISMOESTRATIGRÁFICA DE LA CORTEZA ALREDEDOR DEL KNICKPOINT DE SAN RAFAEL EN EL RÍO COCA, ECUADOR.

Proyecto de investigación previo a la obtención del Título de:

INGENIERA EN GEOCIENCIAS

AUTOR: GARCÍA LÓPEZ ISABEL CRISTINA

TUTOR: PhD. JOSÉ SEBASTIÁN ARAUJO SORIA

Napo - Ecuador

2023

DECLARACIÓN DE DERECHO DE AUTOR, AUTENTICIDAD Y RESPONSABILIDAD

Yo, GARCÍA LÓPEZ ISABEL CRISTINA con documento de identidad N°0805405073, declaro que los resultados obtenidos en la investigación que presento en este documento final, previo a la obtención del título Ingeniero en Geociencias son absolutamente inéditos, originales, auténticos y personales.

En virtud de lo cual, el contenido, criterios, opiniones, resultados, análisis, interpretaciones, conclusiones, recomendaciones y todos los demás aspectos vertidos en la presente investigación son de mi autoría y de mi absoluta responsabilidad.

Tena, 19 de junio de 2023

GARCÍA LÓPEZ ISABEL CRISTINA
C.I. 0805405073

AUTORIZACIÓN DE PUBLICACIÓN EN EL REPOSITORIO INSTITUCIONAL

Yo, ISABEL CRISTINA GARCÍA LÓPEZ, con documento de identidad N°0805405073, en calidad de autor y titular de los derechos morales y patrimoniales del trabajo de titulación: TOMOGRAFÍA SÍSMICA DE TIEMPO DE VIAJE PARA LA INTERPRETACIÓN SISMOESTRATIGRÁFICA DE LA CORTEZA ALREDEDOR DEL KNICKPOINT DE SAN RAFAEL EN EL RÍO COCA, ECUADOR, de conformidad con el Art. 114 del CÓDIGO ORGÁNICO DE LA ECONOMÍA SOCIAL DE LOS CONOCIMIENTOS, CREATIVIDAD E INNOVACIÓN, reconozco a favor de la Universidad Regional Amazónica Ikiam una licencia gratuita, intransferible y no exclusiva para el uso no comercial de la obra, con fines estrictamente académicos.

Así mismo autorizo a la Universidad Regional Amazónica Ikiam para que realice la publicación de este trabajo de titulación en el Repositorio Institucional de conformidad a lo dispuesto en el Art. 144 de la Ley Orgánica de Educación Superior.

Tena, 19 de junio de 2023

Isabel Cristina García López
C.I. 0805405073

CERTIFICADO DE DIRECCIÓN DE TRABAJO DE INTEGRACIÓN CURRICULAR

Certifico que el Trabajo de Integración Curricular Titulado: TOMOGRAFÍA SÍSMICA DE TIEMPO DE VIAJE PARA LA INTERPRETACIÓN SISMOESTRATIGRÁFICA DE LA CORTEZA ALREDEDOR DEL KNICKPOINT DE SAN RAFAEL EN EL RÍO COCA, ECUADOR, en la modalidad de: artículo original, fue realizado por: Isabel Cristina García López, bajo mi dirección.

El mismo ha sido revisado en su totalidad y analizado por la herramienta de verificación de similitud de contenido; por lo tanto, cumple con los requisitos teóricos, científicos, técnicos, metodológicos y legales establecidos por la Universidad Regional Amazónica Ikiam, para su entrega y defensa.

Tena, 19 de junio de 2023

……

José Sebastián Araujo Soria

C.I: 1802672871

AGRADECIMIENTO

Agradezco a mis hermanas y a mi padre José García quienes me han apoyado siempre en mi caminar. Ellos quienes han sido mi mayor motivación. Además, agradezco a mi tía Beatriz García quien me ha ayudado a crecer como persona. Muchas gracias por sus consejos.

Agradezco a mis profesores por su confianza y su guía a través de mis años de estudio. Además, a mis compañeros que me brindaron su compañía y empatía durante mucho tiempo.

DEDICATORIA

Dedico este trabajo a mi Madre que se encuentra con Dios. A mi familia por todo su apoyo. Y a todos que me motivaron a amar a las Geociencias y llegar donde me encuentro.

TABLA DE CONTENIDO

INDICE DE TABLAS

INDICE DE FIGURAS

RESUMEN

Esta investigación tiene como objetivo obtener imágenes tomográficas para interpretar el perfil sismo estratigráfico alrededor del knickpoint de San Rafael mediante tomografía sísmica. La caída de agua de San Rafael en el sumidero del río Coca en febrero de 2020, provocó una erosión regresiva del suelo que sugiere que el knickpoint es altamente inestable. Se utilizó tomografía sísmica para el modelo de velocidad de ondas P basado en catorce estaciones sísmicas de la red sísmica ecuatoriana permanente en la región para obtener secciones transversales verticales con azimut 0, 45º, 90º y 80º. Además, una sección transversal vertical muestra las formaciones geológicas y su transición a los depósitos volcánicos, y una sección transversal horizontal muestra la extensión de los depósitos volcánicos. A partir de las imágenes tomográficas, se identificó la sismoestratigrafía y se correlacionó con la geología de la zona. Los materiales más inestables para la erosión se sitúan entre 0 y 1,5 km con velocidades de hasta 3,5 km/s. El proceso erosivo impacta a la población e infraestructura asentada en las riberas del río Coca con una alta susceptibilidad a la erosión en la zona 1, con velocidades de 3 km/s y una extensión de 10 km. La presa de la CCS se encuentra en la zona 2, con velocidades de 3,8 km/s y una extensión de 40 km con susceptibilidad media a la erosión.

Palabras clave: *Río Coca, knickpoint San Rafael, depósitos volcánicos, erosión, tomografía sísmica.*

ABSTRACT

This research aims to obtain tomographic images to interpret the seismic stratigraphic profile around the San Rafael knickpoint using seismic tomography. The San Rafael waterfall on the Coca River sinkhole in February 2020, caused regressive soil erosion suggesting that the knickpoint is highly unstable. Seismic tomography for the P-wave velocity model based on fourteen seismic stations of the permanent Ecuadorian seismic network in the region were used to obtain vertical cross sections with azimuth 0º, 45º, 90º, and 80º. In addition, a vertical cross-section shows the geological formations and their transition to the volcanic deposits, and a horizontal cross-section shows the extension of the volcanic deposits. From the tomographic images, the seismic stratigraphy was identified and correlated with the geology of the area. The most unstable materials for erosion lie from 0 to 1.5 km with velocities of up to 3.5 km/s. The erosive process impacts the population and infrastructure settled on the banks of the Coca River with a high susceptibility to erosion in zone 1, with velocities of 3 km/s and a 10 km extension. The CCS dam is located in zone 2, with velocities of 3.8 km/s extending up to 40 km with medium susceptibility to erosion.

Keywords: *Coca River, San Rafael knickpoint, volcano deposit, erosion, seismic tomography.*

INTRODUCTION

The modern San Rafael waterfall was formed by a volcaniclastic debris avalanche and lava flow that flowed eastward from the adjacent Reventador volcano. The emplacement of the lava flow caused the Coca River to overtop a high-strength lava barrier whose lava crest line through erosional inputs from the debris avalanche, upper fluvial aggradation, upstream flooding, and overflow of the water flow, causing slowdowns in upstream retreat (Reyes et al., 2021). The basal contact between the lava flow and the underlying debris avalanche deposit was well preserved before the cascade face, reflecting the paleo-level. The composition of the lava flow lies between andesite and basaltic andesite (Sevilla, 1990).

Debris avalanche deposits behind the San Rafael lava dam, fine, non-cohesive matrix sediments of boulders and pebbles would have been carried downward by circulating water, creating an extensive pore network that allowed water to percolate down through the debris avalanche deposit, thus increasing the progressive weakening of the overburden roof in the early 2020s (Reyes et al., 2021).

Through the gradual loss of mechanical support, collapse and a vertical descent of the overburden formed an oval-shaped sinkhole. This catastrophic gravitational collapse led to the immediate abandonment of the San Rafael waterfall. A new interior bypass route was created between the modern alluvial surface, the bottom of the sinkhole, and the excavated arch beneath the uncollapsed lava dam (Reyes et al., 2021).

The rapid retreat of the Coca River cliff was triggered by the formation of the sinkhole following a parallel retreat pattern (Gardner, 1983). Gardner (1983)states that a parallel retreat model must meet three conditions: (1) a resistant upper layer, (2) an underlying level of non-resistant material, and (3) active removal of the underlying material to allow basal scour of the headwall, which meets the conditions of the Coca River erosional process.

Where long periods of slow retreat alternate with short periods of rapid retreat, explaining that the sequence of volcaniclastic sediments is a heterogeneous material with variable resistance to erosion, mainly in the sections of the river upstream of the cascade point (Reyes et al., 2021).

The causes of the regressive erosion process could explain that from May 6 to 9, 2020, almost 2.5km of the slopes and cliffs of the Coca River collapsed. The headward erosion has affected essential infrastructure such as oil pipelines, bridges, and the main road

between Ecuador's capital and oil fields in the Amazon Basin, also, the oil transportation system was the most affected according to the SNGRE (Servicio Nacional de Gestión de Riegos y Emergencias, 2020). Geological and geophysical investigations are indispensable for reducing the risk of the collapse of these infrastructures.

To understand the stratigraphy using seismic data we use travel-time seismic tomography. This method provides the velocity models for the P and S waves and the relocation of the seismic events in the study area. The Corporación Eléctrica del Ecuador (CELEC EP, 2020) conducted low-range seismic and geoelectric studies detecting that most superficial materials correspond to humid and erodible avalanche sediments. However, geophysical methods that can be extended to kilometers at the surface and depth have yet to be performed. The main objective of this research is to obtain tomographic images to interpret the seismic stratigraphic profile around the San Rafael knickpoint. Our research aims to understand the backward erosion geological risk of the dam from Ecuador´s largest hydroelectric power plant Coca Codo Sinclair. In addition, the area's known geology and tectonic structure allow for obtaining a correlation and image interpretation.

STUDY AREA

The study region dimensions are 51.5 km in the WE direction, 49 km in the NS direction, and 40 km in depth in the Coca River basin. The Coca River basin is located in the eastern part of Ecuador with an area of 5283.74 km^2, with an elevation range from 260 to 5.790 masl. The temperature ranges from 18 to 24 ◦C, and its rainfall can reach up to 3000 mm/year. It is known for its rich water resources fed by the Salado and Quijos rivers. The Coca River, flowing northeast, is the largest and most dynamic trunk drainage that receives most of the input from adjacent streams draining from the slopes of the Reventador volcanic edifice (Pourrut et al., 1995). The study area then extends around the upper part Coca River basin with the Reventador volcano as shown in Fig 1.

The Reventador volcano is located in the sub-Andean zone of the Napo uplift. The Napo Uplift presents some volcanic edifices: Reventador, Sumaco, Pan de Azúcar, and Yanaurco. The Reventador volcano is the most active, and its eruptions dictate the geomorphological structure of the region (Barragán & Baby, 2004). The Reventador is a stratovolcano where last significant eruption was in 2002. This eruption had a sub-Plinian activity with VEI 4 (Samaniego et al., 2008). The volcano has had other eruptions that were

less explosive in the years 2004 - 2005 (Samaniego et al., 2008), and the activity continues to this day.

Geology Of The Study Area

The upper part of the Coca River basin is located on an avalanche of debris and sediments accumulated from El Reventador Volcano (Schuster et al., 1996).The outcrops are composed of basaltic lavas, andesites, and dacites. These massive volcanic and volcaniclastic deposits formed in the middle-late Pleistocene to the Holocene depicting the geology around El Reventador volcano (Sevilla, 1990; Tibaldi, 2008). Figure 1 shows the position of the San Rafael knickpoint (red star) in the local and regional contexts and the Coca Codo Sinclair Dam (yellow star). Colors represent the principal geological formations: Holocene fluvial-lacustrine sediments (magenta), Holocene volcanic deposits (blue), 19 ky BP debris avalanche (yellow), Late Pleistocene debris-avalanche (light blue), Misahualli formation (green), Granodiorite intrusions (orange), Volcanic breccias (red), Coca synthem (black), Malo synthem (pink), the arrow also indicates the direction of water flow in the Coca River.

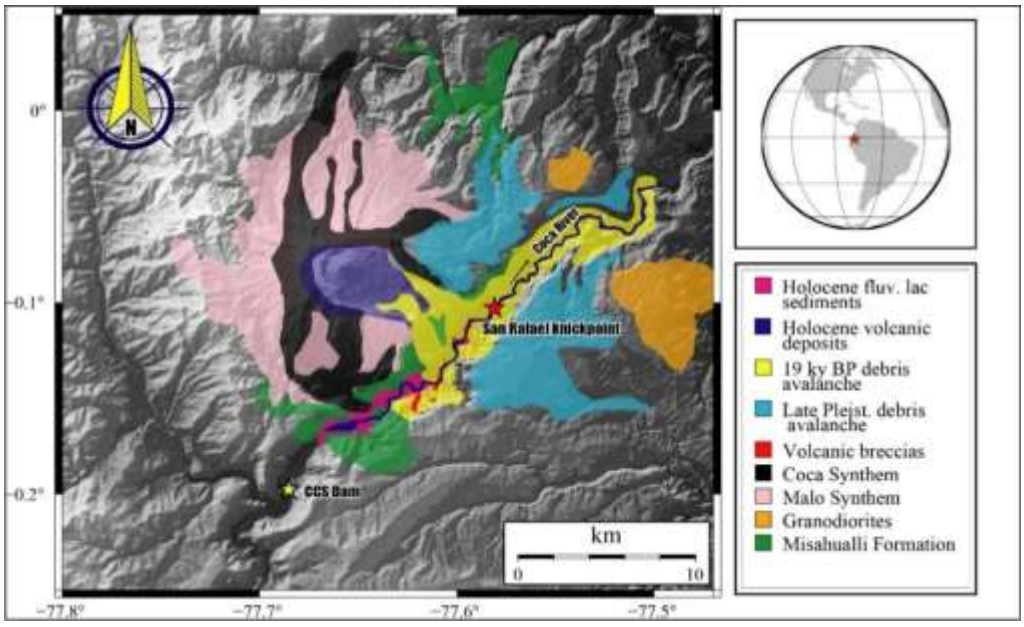

Figure 1: Geological map of the study area. The position of the San Rafael knickpoint with a red star and the Coca Codo Sinclair Dam with a yellow star.
Elaborated By: Garcia, Isabel, 2023
Sources: Contractional tectonics and magma paths in volcano Reventador by Tibaldi 2008. Topographical survey with orthophotography by Kawsus 2020.

In our study region, the Coca River flows through the southern edge of the Reventador volcano cone (IGM, 1988). The position of the knickpoint in the San Rafael waterfall is -77.58ºW, -0.10ºS, at 1189 meters above sea level (Figure 1). The knickpoint was formed when the lava flow from the Reventador volcano blocked the Coca riverbed (Schuster et al., 1996). The Jurassic Misahualli formation composed of welded ash-flow tuffs characterizes the knickpoint zone (INECEL, 1992). On the other hand, the volcanic composition has three differentiated units: The Coca Synthesis of the Pleistocene, the Malo Synthesis of the middle-late Pleistocene, and the Holocene deposits (Tibaldi, 2008). To the east and northeast of the volcano are two granodiorite igneous intrusions (INECEL, 1992; Tibaldi, 2008).

DATA AND STATIONS

The study region has 14 seismic stations of the Ecuadorian Seismic Network RENSIG. The activity survey of the Reventador volcano gives a high number of seismic stations in the zone. The results obtained in the first tomographic inversion over the Ecuadorian region allowed us to relocate the seismicity from 1988 to 2016 in Ecuador (Araujo et al., 2021). Subsequently, the data were completed up to September 2019 with the corresponding catalog. The figure shows the geographical location of the 14 seismic stations (black triangle), knickpoint San Rafael with a red star, and the CCS dam with a yellow star. In addition, the a priori seismicity was observed (yellow dots).

The seismic events were selected inside the tomography box and recorded the 14 stations in the study region, 3212 earthquakes. This selection gives a total of 15487 data to invert, where 11973 are P, and 3514 are S phases. To test the data coverage in all stations, the number of events for each station is depicted in Table 1. For the priori model and seismicity, we use the tomography results from Araujo et al. (2021). For this model, the cell sizes are 5 km x 5 km x 3 km aligned with latitude, longitude, and depth respectively. However, another tomography was made in a smaller box, where the inversion cells are cubes of 0.5 km edge. The number of cells in the box: are 103 in X (east-west), 98 in Y (north-south), and 80 in Z (depth).

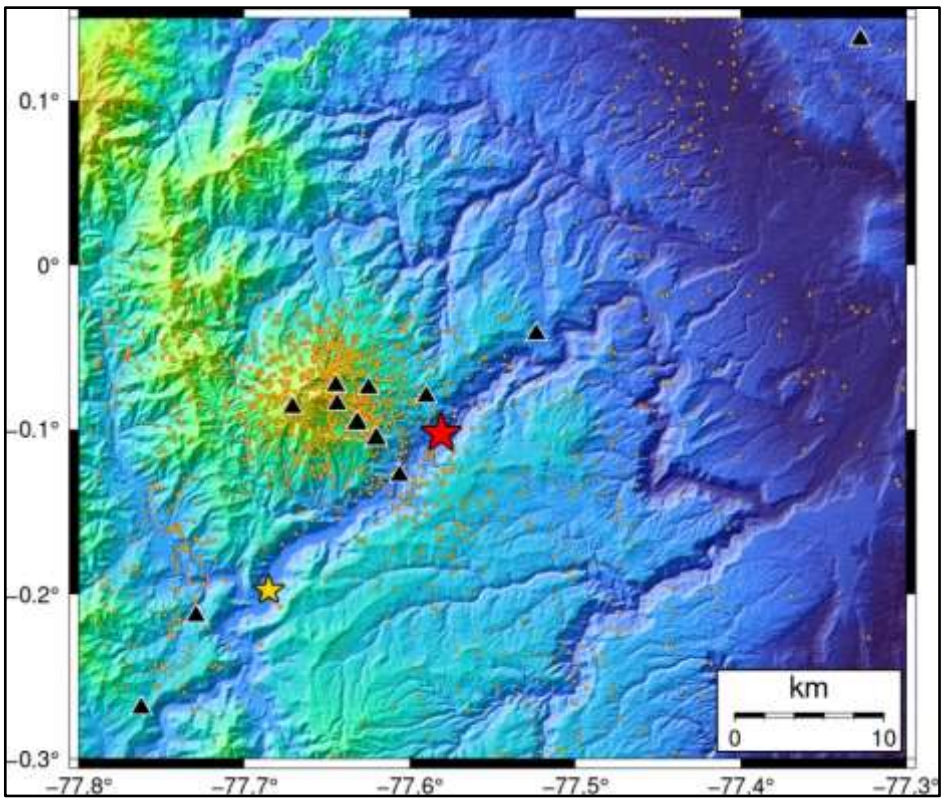

Figure 2: Geographic ubication of the 14 seismic stations
Elaborated By: Garcia, Isabel, 2022

Table 1: Number of P wave phases and S wave phases for each station.

STATION	#P phases	#S phases
AZU1	363	182
BAMB	33	14
CASC	1249	110
CHAR	719	306
CONE	2813	1342
COPE	368	149
LAV2	185	60
LAV3	1092	642
LAV4	1494	209
PALM	398	255
REVE	121	61
REVN	1512	92
REVS	1602	73
TRES	24	19

Elaborated By: Garcia, Isabel, 2022

Tomography Method

We use INSIGHT software (Araujo et al., 2021; Potin, 2016) to obtain seismic tomography images. This software applies the stochastic approach of Valette (2011) to solve the inverse problem that comes from the direct problem equation:

$$\boldsymbol{d_{obs}} = \boldsymbol{g}(\boldsymbol{m}) \tag{1}$$

In equation (1) the data vector $\boldsymbol{d_{obs}}$ contains the travel times of P and S waves, the model vector $\boldsymbol{m}$ have the velocity of the P wave, the ratio between the velocity of P wave velocity and the S wave velocity, the hypocenters and the origin time of the earthquakes. An additional parameter in the model vector is the site effect of each seismic station. The linear operator $\boldsymbol{g}$ is a functional theoretical relation between the data and the parameters.

The stochastic inversion leads to a Tikhonov problem. This problem involves searching for the minimum cost function in a regularization space. The costs function has the form:

$$\left\| \boldsymbol{C_d^{-1/2}} \left(\boldsymbol{d^{obs} - g(m)} \right) \right\|_{\mathbb{D}}^{\boldsymbol{2}} + \left\| \boldsymbol{T(m - m_{prior})} \right\|_{\mathbb{M}}^{\boldsymbol{2}} \quad (2)$$

$\boldsymbol{T}$ is the regularization operator that, in the case of the Gaussian stochastic approach, is the square root of the covariance operator $\boldsymbol{C_m}$ of the model. $\boldsymbol{C_d}$ is the covariance matrix of the data, and the a priori model is $\boldsymbol{m_{prior}}$. To solve this problem numerically, we use the following quasi-Newton algorithm (Tarantola & Valette, 1982):

$$\boldsymbol{m_{k+1} - m_k} = -(\boldsymbol{C_m^{-1} + G_k^* C_d^{-1} G_k})^{-1} \left(\boldsymbol{G_k^* C_d^{-1} (g(m_k) - d_{obs}) + C_m^{-1} (m_k - m_{prior})} \right) \quad (3)$$

Equation (3) can be written using the matrix decomposition described in (Monteiller et al., 2005):

$$\boldsymbol{m_{k+1} - 1} = (\boldsymbol{A_k^* A_k})^{-1} (\boldsymbol{A_k^* A_k}) \quad (4)$$

With formulation (4), the inverse problem is solved using the LSQR algorithm (Paige & Saunders, 1982). For the direct problem, i.e., the ray-tracing, the INSIGHT software uses finite differences (Podvin & Lecomte, 1991).
The decomposition (4) implies the following definitions:

$$\boldsymbol{A_k} = \begin{bmatrix} \boldsymbol{C_d^{-1/2} G_k} \\ \boldsymbol{Cor^{-1/2} \Sigma^{-1}} \end{bmatrix}, \ \boldsymbol{v_k} = \begin{bmatrix} \boldsymbol{C_d^{-1/2} (g(m_k) - d_{obs})} \\ \boldsymbol{Cor^{-1/2} \Sigma^{-1} (m_k - m_{prior})} \end{bmatrix} \text{ and, } \boldsymbol{C_m} = \boldsymbol{\Sigma Cor \Sigma}$$

The introduction of the operators $\boldsymbol{Cor}$ and $\boldsymbol{\Sigma}$ are important because they let us analytically compute the value of $\boldsymbol{C_m^{-1/2}}$. This one avoids the numerical work with the matrix of the model covariance $\boldsymbol{C_m}$ a sparse matrix with many zeros and, therefore, very difficult to invert with traditional methods. The covariance kernel for two points of the inversion grid $\boldsymbol{x}$ and $\boldsymbol{x'}$ with a correlation length $\boldsymbol{\xi}$ and standard deviations $\boldsymbol{\sigma(x)}$ and $\boldsymbol{\sigma(x')}$ is:

$$\boldsymbol{C_m(x, x') = \sigma(x) \sigma(x') exp} \left[\left(\sum_{i=1}^{3} \frac{(x_i - x_i')^2}{\xi_i^2} \right)^{1/2} \right] \quad (5)$$

Where the three indexes for i = 1,2,3 represents the three directions of the space, thus, the covariance kernel takes into account the influence between the points of the grid during the

inversion process. The correlation kernel is defined as $\boldsymbol{Cor}(\boldsymbol{x},\boldsymbol{x'}) = \frac{C_m(x,x')}{\sigma(x)\sigma(x')}$ and Σ the multiplication operator by σ is $(\boldsymbol{\Sigma}\, \boldsymbol{f}) = \boldsymbol{\sigma}(\boldsymbol{x})\boldsymbol{f}(\boldsymbol{x})$.

After being solved, the inverse problem must be regularized. That is, we must choose between the infinite solutions, the optimal solution of the equation (2). The optimal solution expresses the trade-off between the best data fitting $\boldsymbol{d_{obs}} = \boldsymbol{g}(\boldsymbol{m})$ and the most reasonable stabilization $\boldsymbol{m} - \boldsymbol{m_{prior}}$ (Zhdanov, 2015). In the INSIGHT stochastic solution, the value of $(\boldsymbol{m} - \boldsymbol{m_{prior}})(\boldsymbol{x})$ is proportional to the information $\boldsymbol{\sigma}(\boldsymbol{x})^2\boldsymbol{\xi_1}\boldsymbol{\xi_2}\boldsymbol{\xi_3}$ inside a cell of volume $\boldsymbol{\xi_1}\boldsymbol{\xi_2}\boldsymbol{\xi_3}$. Then, the software introduces a renormalization of the model standard deviation σ to be independent of the correlation lengths:

$$\boldsymbol{\sigma} = \frac{\xi_0^3}{\xi_1\xi_2\xi_3}\boldsymbol{\sigma_{phys}} \tag{6}$$

Where the length $\boldsymbol{\xi_0}$ is the characteristic size of the volume of matter for which it is possible to define the standard deviation $\boldsymbol{\sigma_{phys}}$. Then we have all the parameters to regularize the tomography problem: the model standard deviation $\boldsymbol{\sigma_{phys}}$, the correlation o smoothing lengths $\boldsymbol{\xi_{s,}}$, and the attenuation or damping length $\boldsymbol{\xi_0}$. The strategy is to set the standard deviation for the P wave model $\boldsymbol{\sigma_p} = \boldsymbol{0.750m/s}$ and the ratio between P and S wave velocities $\boldsymbol{\sigma_{vp/vs}} = \boldsymbol{0.15}$. It also set the correlations lengths equal in the three space directions $\boldsymbol{\xi_s} = \boldsymbol{\xi_x} = \boldsymbol{\xi_y} = \boldsymbol{\xi_z}$. Then it uses the L-curve criteria (Hansen, 1992) to find the optimization parameters in the vertex of the curve that is $\boldsymbol{\xi_0} = \boldsymbol{3\ km}$ and $\boldsymbol{\xi_0} = \boldsymbol{4\ km}$ (fig. 3)

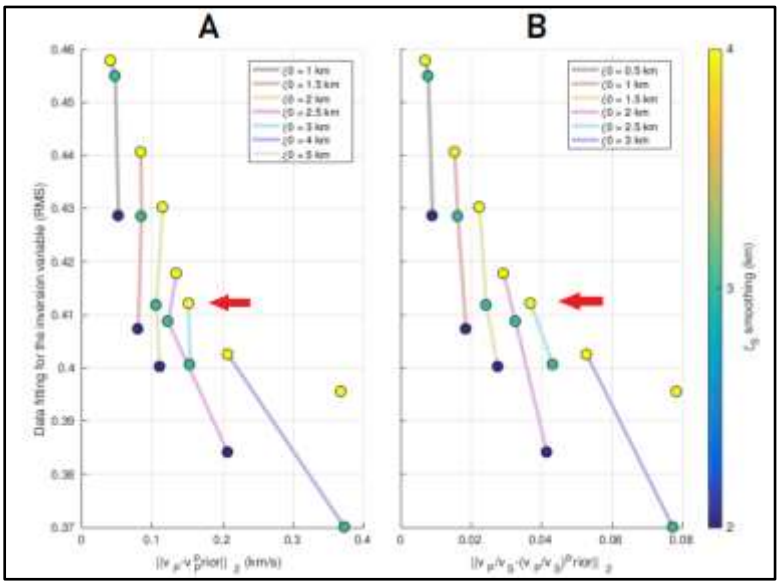

Figure 3: L-curves for the tomography tests. Model A $\boldsymbol{v_P}$, model B $\boldsymbol{v_P/v_S}$.
Elaborated By: Garcia, Isabel, 2022

Regarding the data, one problem that solves the INSIGHT software is the long-tail probability function distribution of the outliers. The solution is to take a hyperbolic secant distribution for the data new variable $\boldsymbol{d}$:

$$\boldsymbol{\rho_{obs}(d)} = \left(\frac{\mathbf{1}}{\mathbf{2}\boldsymbol{\sigma_{obs}}}\right)\frac{\mathbf{1}}{\boldsymbol{cosh}\left(\frac{\boldsymbol{\pi d - d_{obs}}}{\mathbf{2}\ \boldsymbol{\sigma_{obs}}}\right)} \tag{7}$$

With $\boldsymbol{\sigma_{obs}}$ is the error in the data attributed to their quality picking.
The stochastic approach works only with Gaussian probability distributions functions, thus is necessary a new variable definition which is the inversion works:

$$\boldsymbol{y(d)} = \boldsymbol{Er\ f^{-1}}\left[\frac{\mathbf{2}}{\boldsymbol{\pi}}\boldsymbol{arctan}\left(\boldsymbol{sinh}\left(\frac{\boldsymbol{\pi}}{\mathbf{2}}\frac{\boldsymbol{d-d_{obs}}}{\boldsymbol{\sigma_{obs}}}\right)\right)\right] \tag{8}$$

Moreover, the restitution index is evaluated to delimit the volume the resolution of the inversion is certainly very poor. This is a measure of uncertainty in velocity models, which allows for identifying the region where the intersection of seismic rays is sufficiently dense. These values are greater than 0 to 1 for zones with high and low uncertainties. Finally, to obtain reliable results, we analyzed only regions with restitution index values >0.4. While the values with high uncertainty are shaded in white (Vergely et al., 2010).

RESULTS

The tomography cross-sections for the San Rafael knickpoint have three azimuths (fig. 4): 0º, 45º, and 90º. The azimuth 45º follows the Coca River course (fig. 4) and shows the structure out of the Reventador edifice. The seismicity represented in the cross-sections is the relocalizations obtained after the tomography. There are three different models as INSIGHT results: $\boldsymbol{v_P}$ absolute velocity in km/s, the relative velocity: $\Delta\boldsymbol{v_P}$ in percentage from the a priori model, and the $\boldsymbol{v_P/v_S}$ ratio. Each of these three models gives information about the geological structure of the region. In addition, we can add a cut at 80º in the direction of the Reventador volcano.

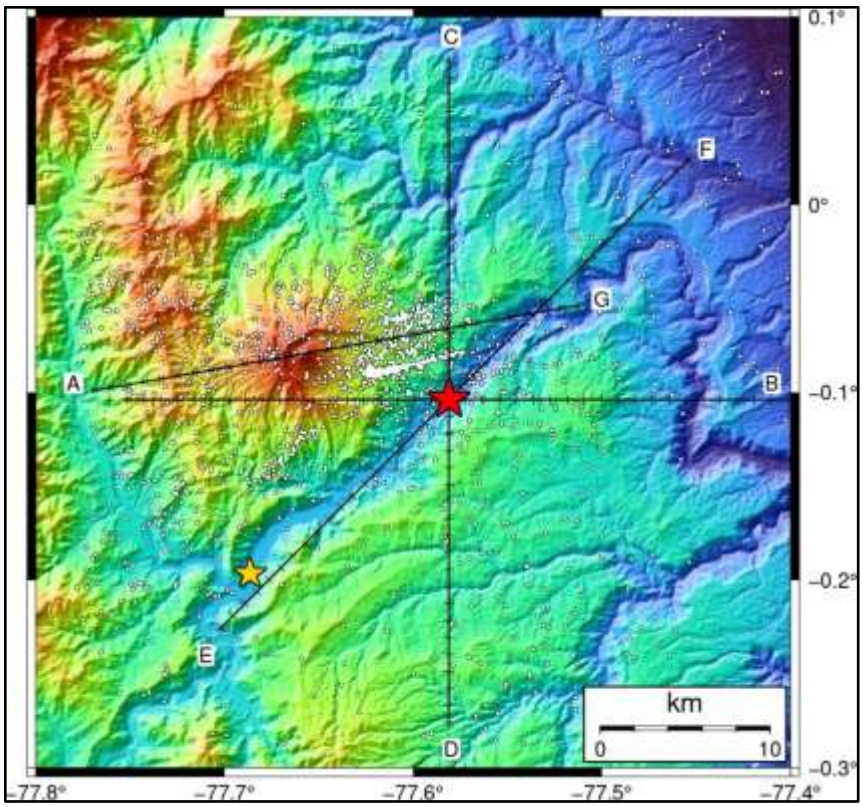

Figure 4: The map of the three tomography cross-sections at the San Rafael contact point (red star), and A of the R volcano.
Elaborated By: Garcia, Isabel, 2023

Cross-Section At Azimuth 0º

Two seismic stratigraphic units can be identified in the DC (0º) cross-section of model A. Unit 1 is located between 1 − 4km depth, here we have values that oscillate between 3.5−4.5 km/s. The thickness of the unit varies from end to end, the first end (D) has a greater thickness than the other end (C). We can observe in the central part (−10 to 5 km) a lateral discontinuity of convex shape upwards (anticline) that comes from unit 2. Unit 2 is located between 4−9 km depth, here we have values between 4.6 − 5.4 km/s.

We can appreciate a lateral discontinuity convex upwards that deforms the material of the unit in the central part, a discontinuity can be observed to the right with less visibility.
However, when observing model B, we can see that the lateral discontinuity of convex (anticline) shape in the central and right part may be other geological structures differing from the surrounding material. The first (central) structure has relative velocity values of 1 − 8%, and the second (B) structure has values ranging from 1 − 4%.
In addition, the surrounding materials are between −30 to 0%. This is a possible interpretation considering that there is a strong thrust regime in the region. Nevertheless,

the anomaly in P wave velocity goes until 4km below the surface, and it is visible in the three cross-sections, that discards the fold interpretation because the anticlines present a preferential folding direction.

Here we can observe the Napo uplift with its different geological formations. In the most superficial part, we have volcanic products of the Reventador, such as avalanche deposits that are between 2 − 3.8 km/s. In addition, these deposits rest on the bedrock of the Misahualli Formation with velocities between 3.8 − 4.5 km/s with a depth between 2 – 5 km deep.

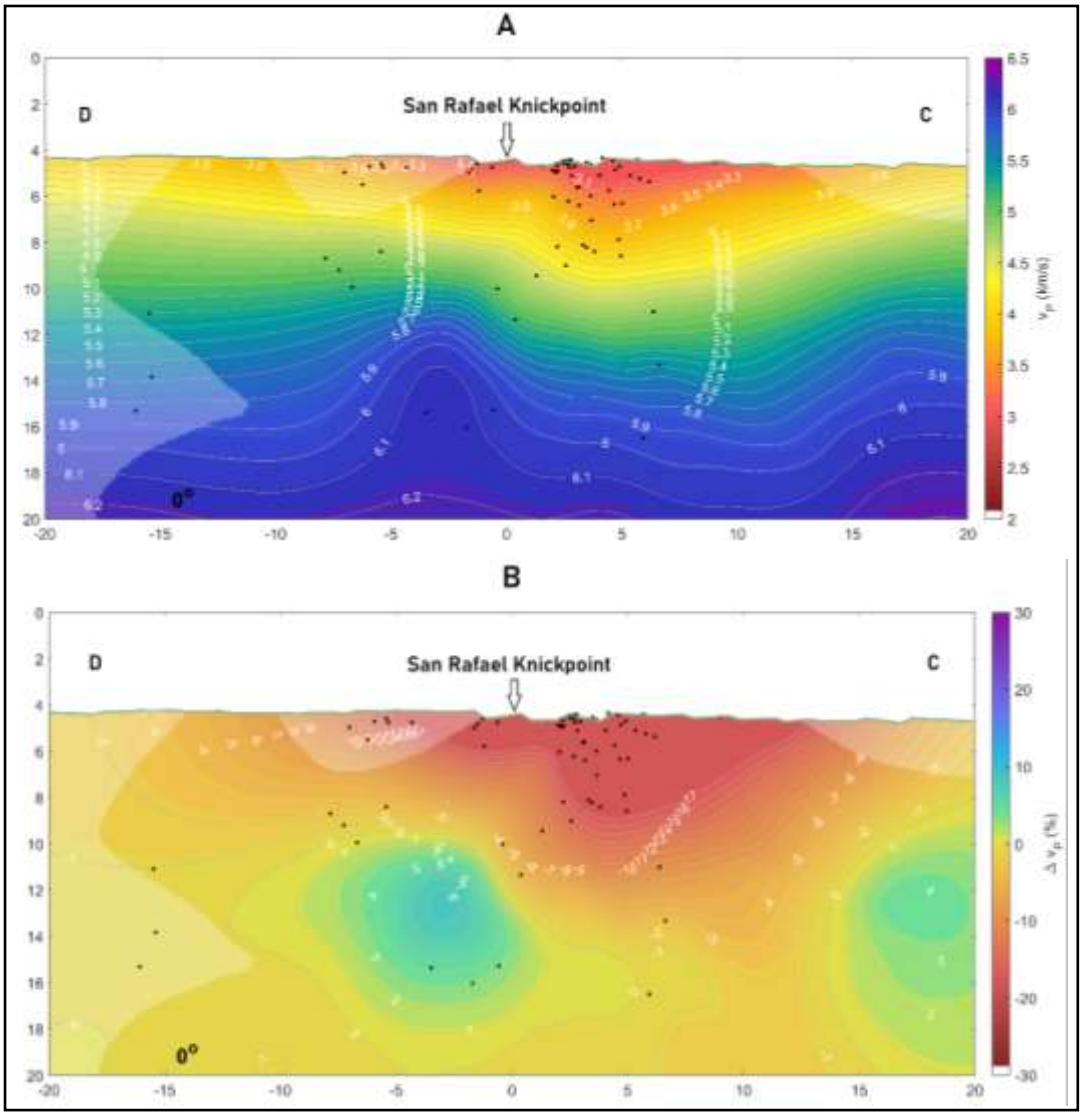

Figure 5: Cross-section with azimuth 0º for the local tomography result. Model A absolute v_P velocity, model B relative Δv_P velocity. Zero position San Rafael knickpoint.
Elaborated By: Garcia, Isabel, 2022

Cross-Section At Azimuth 45º

In the cross-section of 45º, this section is located in the same direction as the Coca River. Here we observe the 2 seismic stratigraphic units with higher visibility of the convex anomalous deformation in the central part of model A. In addition, model B (Δv_P) of −20% are observed in the first 2 km depth in the central part (knickpoint), while the convex anomaly reaches values of 10%.

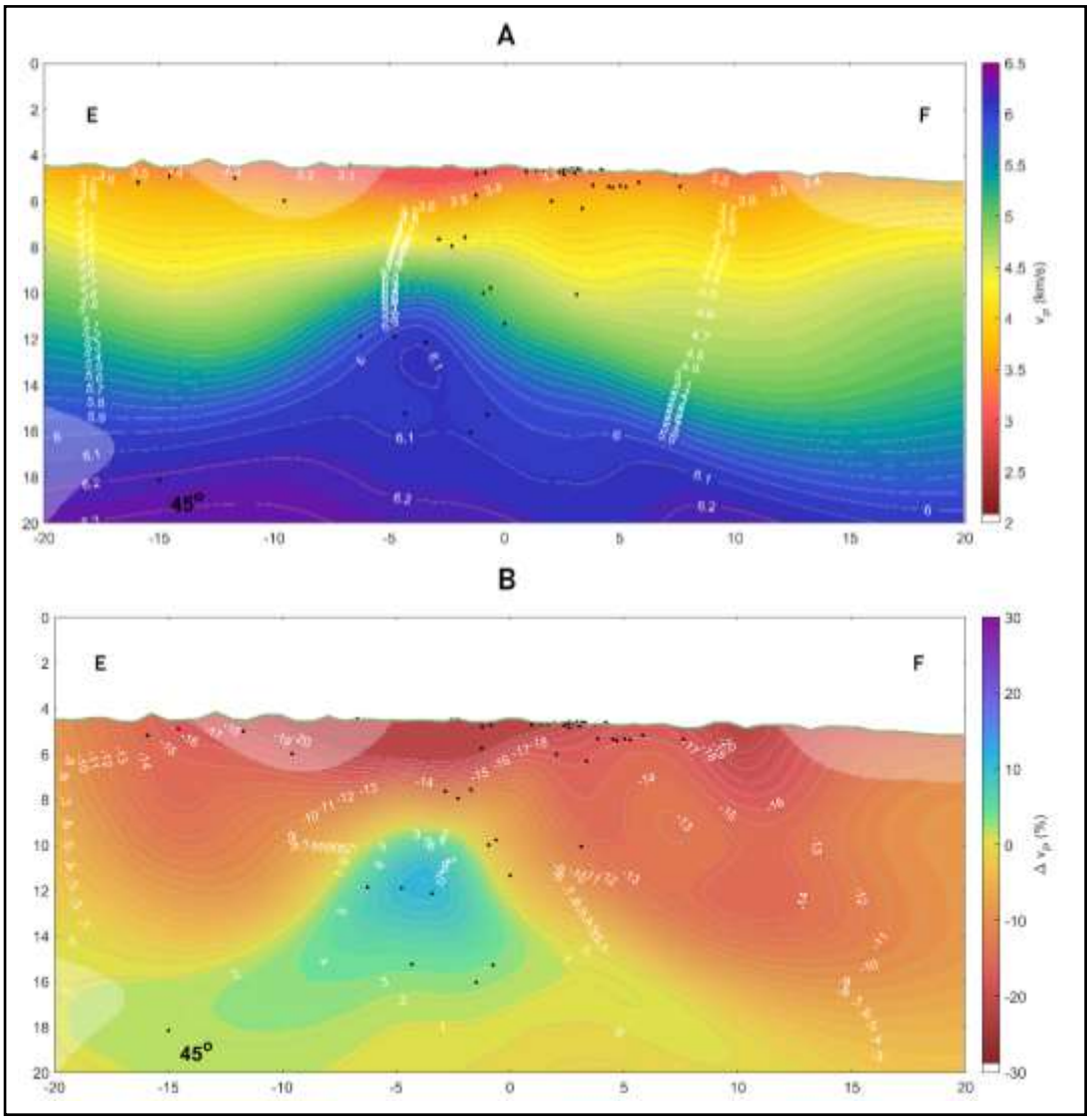

Figure 6: Cross-section with azimuth 45º for the local tomography result. Model A absolute v_P velocity, and model B relative Δv_P velocity.
Elaborated By: Garcia, Isabel, 2022

Cross-Section At Azimuth 90º

The cross-section of model A covers the southern part (left) of the Reventador volcano. Here we can observe velocities of 2.5 km/s up to 3 km depth. These velocities are from volcanic deposits derived from the volcano. The relative velocity model of the P wave Δv_P helps to clarify the anomaly observed in the absolute v_P images. Here we can observe a volumetric structure defined by $\Delta v_P \geq +10\%$ and highlighted by the red color in the figures (6 - model B). This structure is approximately 8 km long in the NS direction, 5 km long in the WE direction, and 5 km depth below the surface.

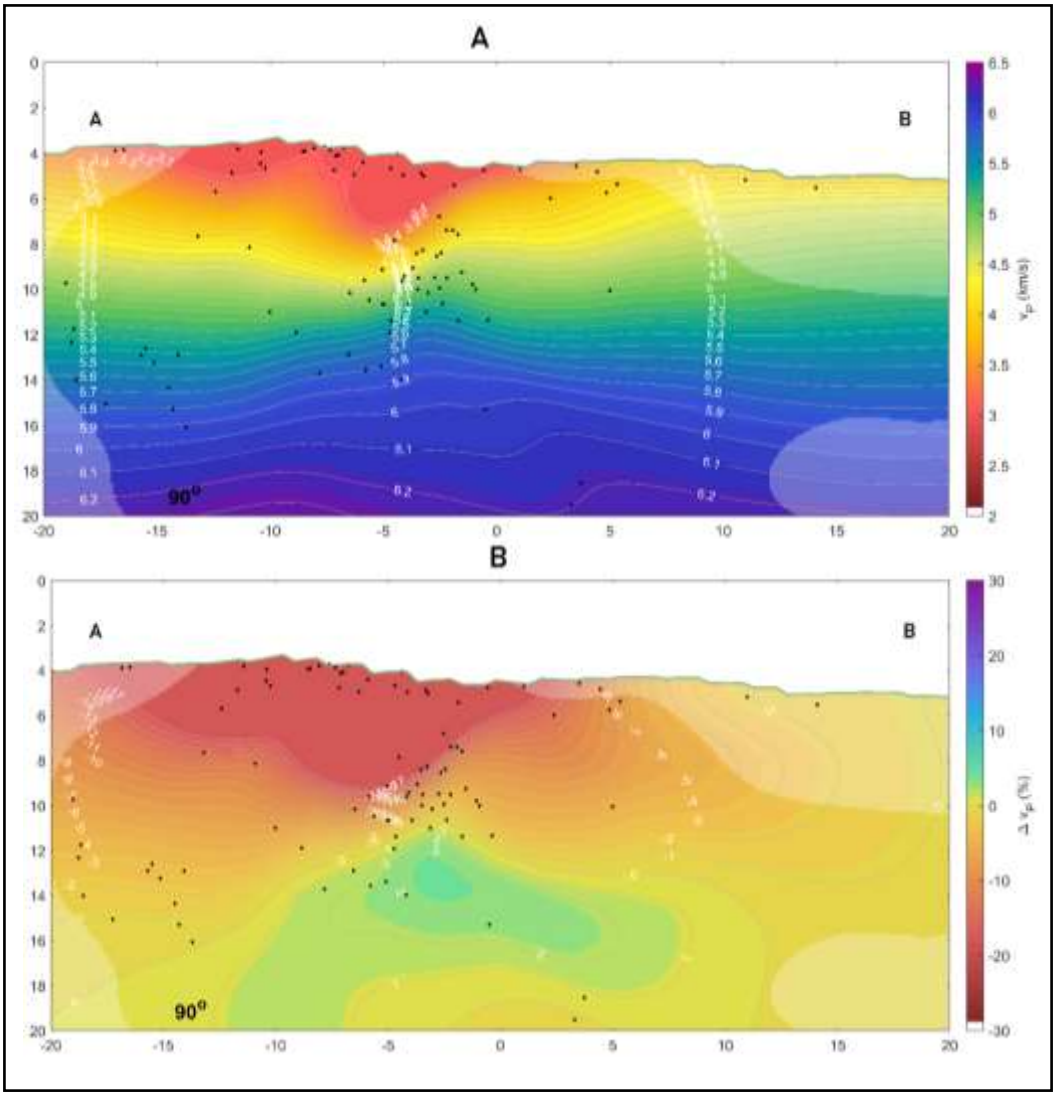

Figure 7: Cross-section with azimuth 90º for the local tomography result. Model A absolute v_P velocity, and model B relative Δv_P velocity.
Elaborated By: Garcia, Isabel, 2022

In the three cross-sections, we can observe regions with high uncertainty that are shaded in white. In these places, it is not possible to obtain a certain result but a guess according

to the results with low uncertainty. These uncertainties are caused by the lack of seismic information due to the position of the seismic stations that are distributed almost all around the volcano.

The Horizontal Cross-Section In The Study Area

Figure 8 shows the horizontal slice of the volcanic deposits produced by its proximity to the Reventador volcano. We present the v_P model and the relative velocity model Δv_P. Here we can observe the shape and extent of the volcanic deposits and the possible materials that have eroded and possibly will erode. In the v_P in the direction of the knickpoint, we have velocities of 2.5 – 3 km/s. While in the Δv_P we have an oval-shaped extension ranging from −40 to −12% with a length of approximately 40 km.

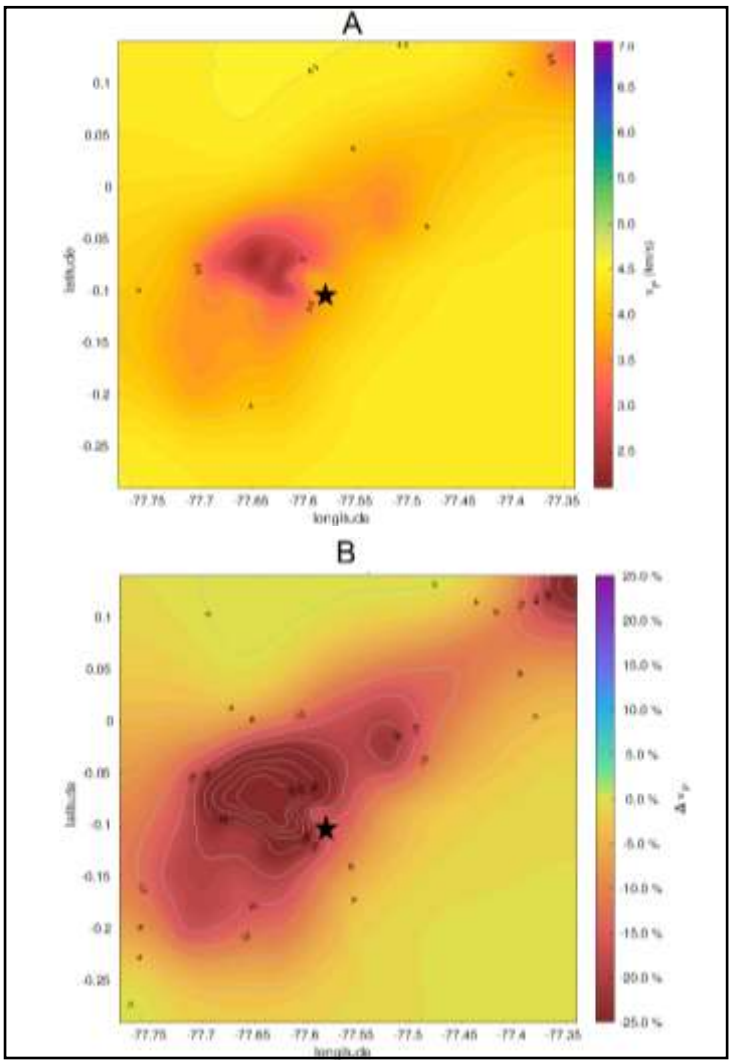

Figure 8: Horizontal slices below the surface of the v_P absolute velocity (A) and the Δv_P relative velocity (B).
Elaborated By: Garcia, Isabel, 2022

Cross-Section At Azimuth 80º

In addition, it was possible to perform the tomographic cross-section at 80º to the east of the Reventador volcano, since the relocation of the seismic obtained by INSIGHT is essential at this location as shown in Figure 4. After the re-localization, the earthquakes define a structure almost vertical 12 km depth below the surface (fig. 9). The resulting model B shows also a deeper magmatic chamber 15 km to the east and 25 km depth defined by a high value of the velocities ratio v_P/v_S= 1.7.

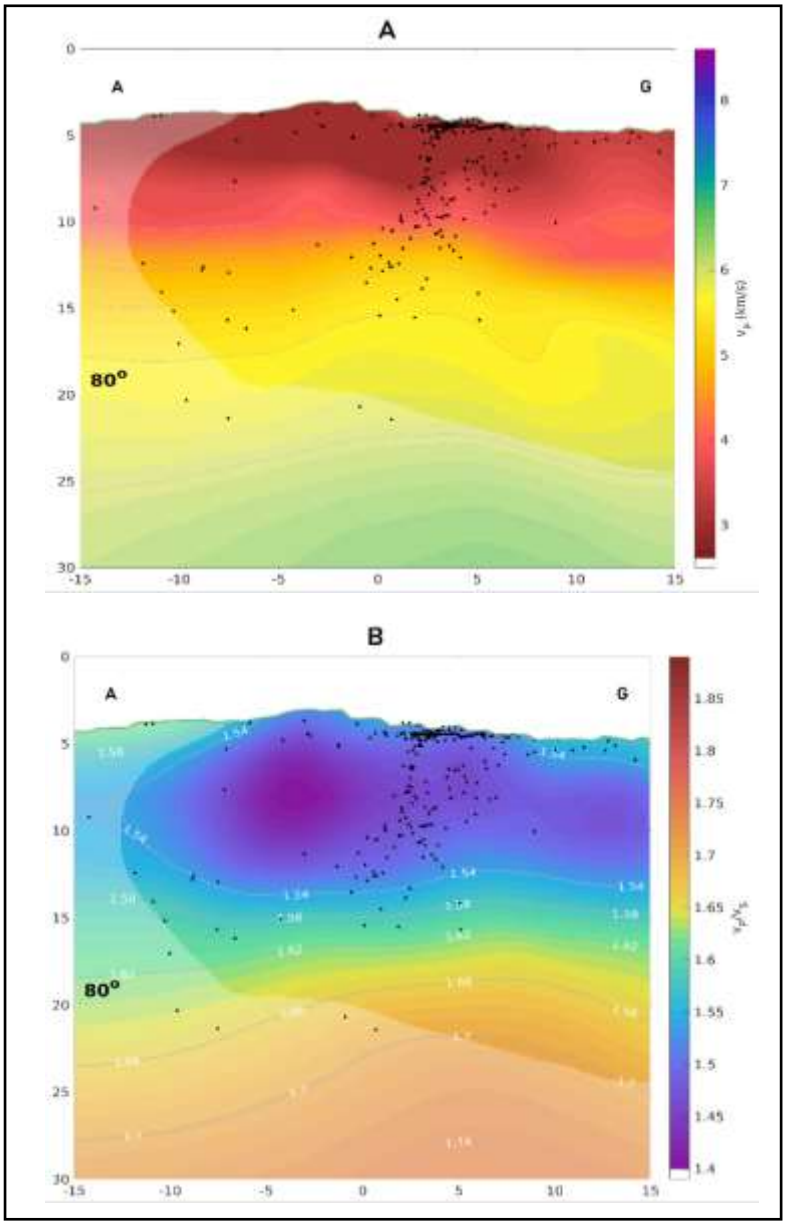

Figure 9: Cross-section with azimuth 80º. Absolute v_P velocity model A, and ratio v_P/v_S velocity model B (Km=scale).
Elaborated By: Garcia, Isabel, 2022

DISCUSSION

According to the results, the study area has a high instability which indicates a high susceptibility to erosion. The seismic stratigraphic interpretation is carried out from the oldest to the most recent geological events (fig. 10). An igneous intrusion is centered at San Rafael Knickpoint below Unit 2 at a depth of 10 km in hard rock. There is evidence of another two intrusions of the same type in the region (see Fig. 1) to 10km NE.

The previous geological studies (INECEL, 1992; Tibaldi, 2008) do not show evidence of this intrusion, probably because it is recovered with the debris avalanche of Reventador. However, seismic tomography studies show these plutons in many geological contexts, e.g., in the Iberian Massif (Spain), the granitic plutons are detected by 2D reflection seismic tomography with velocities $v_P \geq 5.5$ km/s (Flecha et al., 2006). In the Ngatamarki geothermal field in New Zealand, the diorite plutons are identified using seismic travel-time tomography with velocities v_P = 5.5 – 6 km/s and relative velocity Δv_P= +15%; in this volcanic zone, plutons do not reach the surface and are 5−10 km deep (Sherburn et al., 2003).

Another reason to favor the granodioritic intrusion as an explanation for the high v_P anomaly found in our tomography survey, it is that volcanic activity in a compressional tectonic realm as the Reventador volcano (Tibaldi, 2005) produces granite magma migration and its emplacement in the form of plutons which has can be demonstrated by the Reventador volcano using an analogical model (Ferré et al., 2012). This igneous intrusion has a power of 8 km and produces convex deformation in the zone below the knickpoint, allowing the overlying materials to deform and the more recent materials to become unstable as they consolidate.

Unit 2 would be comprised of the Santiago Formation (thickness ranging from 1.5 to 2.7 km). This formation consists of thin-bedded black siliceous limestones alternating with calcareous sandstones and sometimes bituminous black shales (Tschopp, 1953). This formation is compact and not susceptible to erosion and has a convex deformation caused by igneous intrusion beneath it, and is in stratigraphic contact below the Misahualli Formation. This cycle is syn-tectonic and records the opening of a "Rift" (Christophoul et al., 1999), evidenced by continental tholeiitic volcanism (Romeuf et al., 1995), and is related to the Tetian opening that influenced the evolution of the Northern Andes (Jaillard et al., 1990).

Unit 1 we have the Misahualli Formation in direct contact with the volcanic materials laying above this formation (erodible materials). Being in contact with the Santiago Formation, this also has a convex deformation causing instability of the erodible volcanic materials. This formation outcrops at -15 km (fig 10, SSW), this outcrop is the last non-erodible layer. The Misahualli formation thickness usually ranges from 1 to 4 km (Tschopp, 1953), and we obtain 3.5 km in our tomography result. This interpretation matches the geological background of the region where the Jurassic Misahualli formation is the basement of the Coca River course (INECEL, 1992).

Tschopp (1953) defined the Misahualli Formation as an upper member of the Chapiza Formation. The Misahualli Formation is a geological formation of tuffs and basalts, very hard rocks. Therefore, Misahualli and the Chapiza Formations are taken as unit 1 in Figure 10. The Misahualli Formation consists of volcanic accumulations, and intrusions (J. Aspden et al., 1990; J. A. Aspden & Litherland, 1992; Romeuf et al., 1995). The geodynamic event terminates the opening of the "Rift" ("Aborted Rift"), which causes uplift and emersion of the "Rift", resulting in the erosional surface of the base of the Chapiza Fm. (Christophoul et al., 1999).The continental Chapiza Fm. is contemporaneous with the Misahualli volcanic arc of continental origin (Baby et al., 2004).

In the study area, we have the deposits of the Reventador volcano that are currently eroding. These deposits are on top of Unit 1 composed of gravitational debris avalanches and water flows that settled in this place. Erodible materials are dacites, andesites, and rhyolites interrupted by basaltic lavas at the knickpoint (Tibaldi, 2008).

The collapse of the San Rafael cascade starts with the transport of avalanche deposits below the lava flow. This process relied on the weakly resistant materials of the volcanic deposits leaving newly abandoned alluvial terrace plains in the downstream reaches. Whereas, upstream of the knickpoint the erosional process showed a non-constant rate of retreat, suggesting that the volcanic deposit, despite its loose nature, exhibited a strong internal heterogeneity (Reyes et al., 2021). Figure 11 of Zone 1 (black lines) shows velocities <3.5 km/s over a distance of 10 km. This zone is very close to the knickpoint (black star) indicating a high susceptibility to erosion as low velocities (< 3.5 km/s) indicate looser materials.

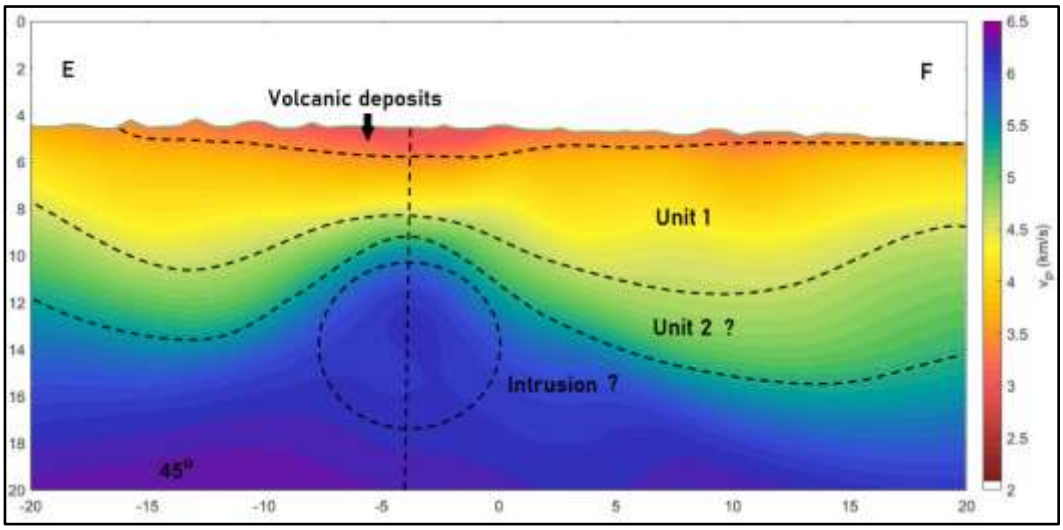

Figure 10: Seismic stratigraphic interpretation of the 45º cross-section. The seismic stratigraphic units are identified in the central part of the line (-5 km left).
Elaborated By: Garcia, Isabel, 2023

Furthermore, it is expected that backward erosion will reach the point of the Coca Codo Sinclair Dam. However, predicting when the erosion will reach the dam is uncertain because the erodible material are heterogeneous and the backward velocity vary depending on factors such as geology, stratigraphic, tectonics, and seismic that can accelerate or slow down the erosion process (Reyes et al., 2021). Figure 11 shows that the CCS dam (green star) is located where the velocity changes from 3.5 to 3.8 km/s, which indicates a medium susceptibility to erosion. Besides, the CCS dam, human settlements, roads, pipelines, and other infrastructure will be damaged due to backward erosion (Reyes et al., 2021).

The regressive erosion is enhanced in the main impact zone located approximately 100m from the community of San Luis, where the risk of slope instability is high. In addition, the erosion front is located at a distance of 7.9 km from the CCS Dam, it remains in the zone of medium susceptibility to erosion according to Dirección de Monitoreo de Eventos Adversos (2022).

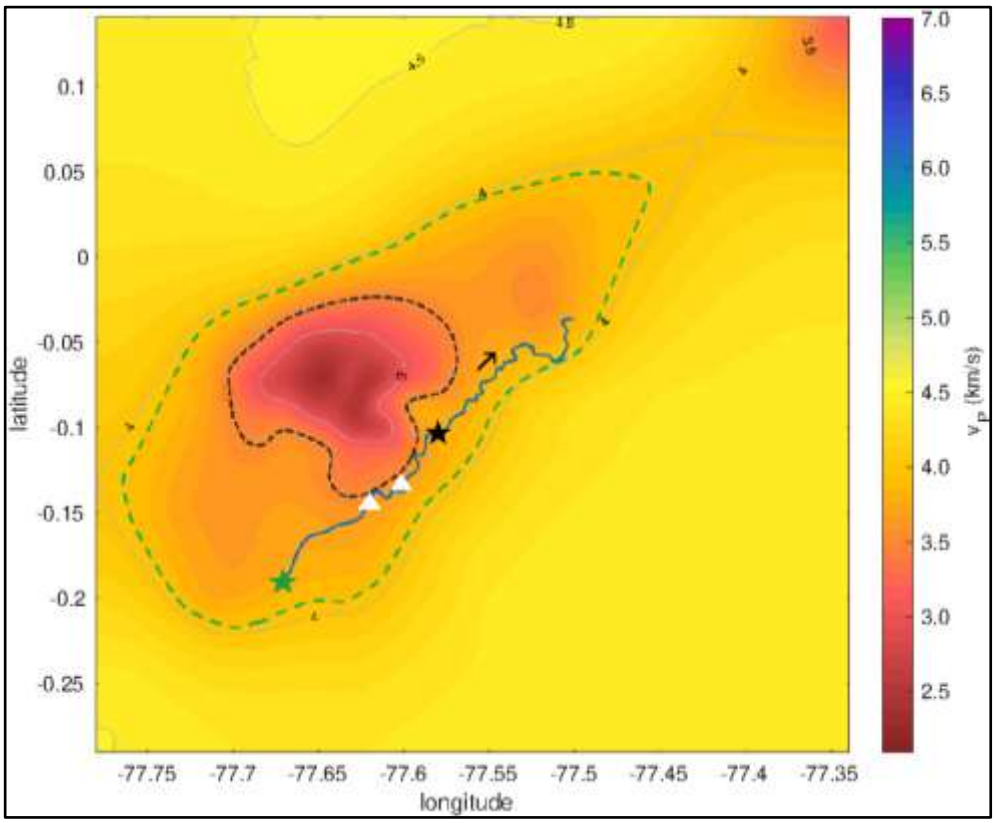

Figure 11: Extent of volcanic deposits. The knickpoint position (black star). The CCS dam (green star). The Coca River with a blue line.
Elaborated By: Garcia, Isabel, 2022

In addition, a cross-section that passes through the Reventador volcano was analyzed (Figure 9), in this area, allows to obtain seismic stratigraphic data. This activity may indicate an active feeding system of the volcano through faults with a depth of 10 km. However, the seismic activity in the Reventador volcano is characterized by a high number of tectonic and volcano-tectonic events that make it difficult to separate these two phenomena (Hall et al., 2004). Some precursory earthquakes were localized to the SW of the volcano before the paroxysmal eruption in November 2002 (Hall et al., 2004). Like other active volcanoes, The Reventador seismic recurrence produces tremors and explosions at irregular intervals favoring landslides in the area (Lees et al., 2008).

CONCLUSIONS

The tomographic images provided insight into the geology and structures beneath the San Rafael knickpoint, allowing the strata identification and correlation with the geology of the area. The tomographic analysis allowed the identification of unstable materials highly susceptible to erosion at a depth from 0 to 1.5 km with velocities of up to 3.5 km/s.

In addition, the igneous intrusion was detected below the SR knickpoint, which allowed the deformation of Santiago and Misahualli's geological formations, resulting in instability in the area.

The erosion process impacts the population and essential infrastructure settled along the banks of the Coca River with a high susceptibility to erosion in zone 1, with velocities of 3 km/s has an extension of 10 km. It can be expected that the regressive erosion will eventually reach the CCS Dam, that lies on a region with unconsolidated volcanic deposits, with velocities of 3.8 km/s that are susceptible to erosion.

Another factor that allows instability for the regressive erosion process in the area is the high seismicity of the Reventador volcano.

BIBLIOGRAPHY

Araujo, S., Valette, B., Potin, B., & Ruiz, M. (2021). A preliminary seismic travel time tomography beneath Ecuador from data of the national network. *Journal of South American Earth Sciences*, *111*, 103486. https://doi.org/10.1016/j.jsames.2021.103486

Aspden, J. A., & Litherland, M. (1992). The geology and Mesozoic collisional history of the Cordillera Real, Ecuador. *Tectonophysics*, *205*(1–3), 187–204. https://doi.org/10.1016/0040-1951(92)90426-7

Aspden, J., Rundle, C., Viteri, F., Bermudez, R., & Harrison, S. (1990). Edades radiométricas del Batolito de Zamora-rio Mayo. *Boletín Geológico Ecuatoriano*, *1*(1), 85–88.

Baby, P., Rivadeniera, M., & Barragán, R. (2004). La cuenca Oriente: geología y petróleo (Vol. 144). In Patrice Baby, M. Rivadeneira, & R. Barragán (Eds.), *Institut français d'études andines*. .

Barragán, R., & Baby, P. (2004). Evolución magmática actual de la zona subandina: volcanes el Reventador y Sumaco, modelos geodinámicos preliminares. *La Cuenca Oriente: Geología y Petróleo*, 183–201.

CELEC EP. (2020). *Investigación Del Subsuelo Con Métodos De Geofísica, en el tramo entre el salado y la Cascada San Rafael, debido a la erosión regresiva en el Río Coca*.

Christophoul, F., Baby, P., & Dávila, C. (1999). *Descripción de las influencias eustáticas y tectónicas en la Cuenca Oriente ecuatoriana desde el Aptiano hasta el Oligoceno*.

Dirección de Monitoreo de Eventos Adversos. (2022, July 15). *Informe de Situación No. 68 Erosión Hídrica Regresiva en el tramo fluvial: Hidroeléctrica Coca Codo Sinclair – Río Napo*. https://www.gestionderiesgos.gob.ec/wp-content/uploads/downloads/2022/07/SITREP-No-68-Erosion-Hidrica-NapoOrellana-15072022.pdf

Ferré, E. C., Galland, O., Montanari, D., & Kalakay, T. J. (2012). Granite magma migration and emplacement along thrusts. *International Journal of Earth Sciences*, *101*(7), 1673–1688. https://doi.org/10.1007/s00531-012-0747-6

Flecha, I., Carbonell, R., Zeyen, H., Martí, D., Palomeras, I., Simancas, F., & Pérez-Estaún, A. (2006). Imaging granitic plutons along the IBERSEIS profile. *Tectonophysics*, *420*(1–2), 37–47. https://doi.org/10.1016/j.tecto.2006.01.019

Gardner, T. W. (1983). Experimental study of knickpoint and longitudinal profile evolution in cohesive, homogeneous material. *Geological Society of America Bulletin*, *94*(5), 664. https://doi.org/10.1130/0016-7606(1983)94<664:ESOKAL>2.0.CO;2

Hall, M., Ramón, P., Mothes, P., LePennec, J. L., García, A., Samaniego, P., & Yepes, H. (2004). Volcanic eruptions with little warning: the case of Volcán Reventador's Surprise November 3, 2002 Eruption, Ecuador. *Revista Geológica de Chile*, *31*(2). https://doi.org/10.4067/S0716-02082004000200010

Hansen, P. (1992). Analysis of discrete ill-posed problems by means of the L-curve. *SIAM Review*, *34*(4), 561–580.

IGM. (1988). *Carta Topográfica: Atenas, Escala 1:50.000 (CT-OIII-B1)*.

INECEL. (1992). *Anexo G (Vulcanología).Estudio de Factibilidad del Proyecto Hidroeléctrico Coca Codo Sinclair - Fase B.*

Jaillard, E., Soler, P., Carlier, G., & Mourier, T. (1990). Geodynamic evolution of the northern and central Andes during early to middle Mesozoic times: a Tethyan model. *Journal of the Geological Society*, *147*(6), 1009–1022. https://doi.org/10.1144/gsjgs.147.6.1009

Kawsus. (2020). *Informe final: contrato de consultoría para levantamiento topográfico con ortofotografia – lidar y diagnostico geológico geotécnico de erosión del lecho del río Coca*.

Lees, J. M., Johnson, J. B., Ruiz, M., Troncoso, L., & Welsh, M. (2008). Reventador Volcano 2005: Eruptive activity inferred from seismo-acoustic observation. *Journal of Volcanology and Geothermal Research*, *176*(1), 179–190. https://doi.org/10.1016/j.jvolgeores.2007.10.006

Monteiller, V., Got, J., Virieux, J., & Okubo, P. (2005). An efficient algorithm for double-difference tomography and location in heterogeneous media, with an application to the Kilauea volcano. *Journal of Geophysical Research: Solid Earth*, *110*(B12).

Paige, C. C., & Saunders, M. A. (1982). Algorithm 583: LSQR: Sparse Linear Equations and Least Squares Problems. *ACM Transactions on Mathematical Software*, *8*(2), 195–209. https://doi.org/10.1145/355993.356000

Podvin, P., & Lecomte, I. (1991). Finite difference computation of traveltimes in very contrasted velocity models: a massively parallel approach and its associated tools. *Geophysical Journal International*, *105*(1), 271–284. https://doi.org/10.1111/j.1365-246X.1991.tb03461.x

Potin, B. (2016). *). Les Alpes occidentales: tomographie, localisation de séismes et topographie du Moho (Doctoral dissertation, Grenoble Alpes).*

Pourrut, P., Gomez, G., & Segovia, A. (1995). *El agua en el Ecuador: clima, precipitaciones, escorrentía.*

Reyes, P., Procel, S., Sevilla, J., Cabero, A., Orozco, A., Córdova, J., Lima, F., & Vasconez, F. (2021). Exceptionally uncommon overburden collapse behind a natural lava dam: Abandonment of the San-Rafael Waterfall in northeastern Ecuador. *Journal of South American Earth Sciences*, *110*, 103353. https://doi.org/10.1016/j.jsames.2021.103353

Romeuf, N., Aguirre, L., Soler, P., Feraud, G., Jaillard, E., & Ruffet, G. (1995). Middle Jurassic volcanism in the Northern and Central Andes. *Revista Geológica de Chile*, *22*(2), 245–259.

Samaniego, P., Eissen, J.-P., Le Pennec, J.-L., Robin, C., Hall, M. L., Mothes, P., Chavrit, D., & Cotten, J. (2008). Pre-eruptive physical conditions of El Reventador volcano (Ecuador) inferred from the petrology of the 2002 and 2004–05 eruptions. *Journal of Volcanology and Geothermal Research*, *176*(1), 82–93. https://doi.org/10.1016/j.jvolgeores.2008.03.004

Schuster, R. L., NietoThomas, A. S., D. O'Rourke, T., Crespo, E., & Plaza-Nieto, G. (1996). Mass wasting triggered by the 5 March 1987 ecuador earthquakes. *Engineering Geology*, *42*(1), 1–23. https://doi.org/10.1016/0013-7952(95)00024-0

Sevilla, J. (1990). Un exemple d'importants glissements de terrain en Equateur. *Int. Congr. Int. Assoc*, 1713–1717.

Sherburn, S., Bannister, S., & Bibby, H. (2003). Seismic velocity structure of the central Taupo Volcanic Zone, New Zealand, from local earthquake tomography. *Journal of Volcanology and Geothermal Research*, *122*(1–2), 69–88. https://doi.org/10.1016/S0377-0273(02)00470-5

SNGRE. (2020). *Informe de Situación – Socavamiento Napo*.

Tarantola, A., & Valette, B. (1982). Generalized nonlinear inverse problems solved using the least squares criterion. *Reviews of Geophysics*, *20*(2), 219. https://doi.org/10.1029/RG020i002p00219

Tibaldi, A. (2005). Volcanism in compressional tectonic settings: Is it possible? *Geophysical Research Letters*, *32*(6), L06309. https://doi.org/10.1029/2004GL021798

Tibaldi, A. (2008). Contractional tectonics and magma paths in volcanoes. *Journal of Volcanology and Geothermal Research*, *176*(2), 291–301. https://doi.org/10.1016/j.jvolgeores.2008.04.008

Tschopp, H. (1953). Oil Explorations in the Oriente of Ecuador, 1938-1950. *AAPG Bulletin*, *37*. https://doi.org/10.1306/5CEADD94-16BB-11D7-8645000102C1865D

Valette, B. (2011). *Inversion of geophysical data. In EFIDIR: Extraction and Fusion of Information for Displacement measurement from SAR Imagery*. Ecole de Physique Des Houches, Chamonix. . http://efidir.poleterresolide.fr/index.php/efidir-seminars/spring-school-2011

Vergely, J.-L., Valette, B., Lallement, R., & Raimond, S. (2010). Spatial distribution of interstellar dust in the Sun's vicinity. *Astronomy and Astrophysics*, *518*, A31. https://doi.org/10.1051/0004-6361/200913962

Zhdanov, M. (2015). *Inverse theory and applications in geophysics* (Vol. 36). Elsevier.